ARTICLE IN PRESS [m5+;February 16, 2024;14:7

FISEVIER

Available online at www.sciencedirect.com

ScienceDirect

Journal of Magnesium and Alloys xxx (xxxx) xxx



www.elsevier.com/locate/jma

Full Length Article

Transmutation of zonal twinning dislocations during non-cozone {1011} twin-twin interaction in magnesium

Peng Chen^{a,*}, Bin Li^{b,*}

^a Key Laboratory of Automobile Materials (Ministry of Education) and School of Materials Science and Engineering, Jilin University, Changchun 130022, China

> ^b Department of Industrial and Manufacturing Systems Engineering, Iowa State University, Ames, USA Received 19 October 2023; received in revised form 30 December 2023; accepted 23 January 2024 Available online xxx

Abstract

Theoretically, a twinning dislocation must stay on the twinning plane which is the first invariant plane of a twinning mode, because the glide of twinning dislocation linearly transforms the parent lattice to the twin lattice. However, recent experimental observations showed that a $\{10\bar{1}1\}\langle10\bar{1}2\rangle$ twin variant could cross another variant during twin-twin interaction. It is well known that $\{10\bar{1}1\}$ twinning is mediated by zonal twinning dislocations. Thus, how the zonal twinning dislocations transmute during twin-twin interaction is of great interest but not well understood. In this work, atomistic simulation is performed to investigate interaction between $\{10\bar{1}1\}$ twin variants. Our results show that when an incoming twin variant impinges on the other which acts as a barrier, surprisingly, the barrier twin can grow at the expense of the incoming twin. Eventually one variant consumes the other. Structural analysis shows that the twinning dislocations of the barrier variant are able to penetrate the zone of twin-twin intersection, by plowing through the lattice of one variant and transform its lattice into the lattice of the other. Careful lattice correspondence analysis reveals that, the lattice transformation from one variant to the other is close to $\{10\bar{1}2\}\langle10\bar{1}\bar{1}\rangle$ twinning, but the orientation relationship deviates by a minor lattice rotation. This deviation presents a significant energy barrier to the lattice transformation, and thus it is expected such a twin-twin interaction will increase the stress for twin growth.

© 2024 Chongqing University. Publishing services provided by Elsevier B.V. on behalf of KeAi Communications Co. Ltd.

This is an open access article under the CC BY-NC-ND license (http://creativecommons.org/licenses/by-nc-nd/4.0/)

Peer review under responsibility of Chongqing University

Keywords: Magnesium; Contraction twinning; Atomistic simulation; Lattice transformation.

1. Introduction

Twin-twin interaction occurs when multiple twin variants are activated in a crystal and has been extensively investigated in cubic metals [1–6]. When an incoming twin impinges on a pre-existing twin (barrier twin), several scenarios may occur: (1) the incoming twin interacts with the barrier twin by generating a secondary twin at the intersection [2–4]; (2) the incoming twin is impeded by the barrier twin at the intersection [5]; (3) the twinning dislocation of the incoming twin is incorporated into the barrier twin by complex dislocation reactions [1,6,7]. According to Rémy [8], the incorporation of

E-mail addresses: pchen21@jlu.edu.cn (P. Chen), binl@iastate.edu (B. Li)

the incoming twinning dislocation into a barrier twin boundary could generate a step or glide ledge at the interface and the shear stress is released: (1) by dislocation slip in the incoming twin and barrier twin; (2) solely by dislocation slip in the barrier twin; (3) partly by secondary twinning of the barrier twin and partly by slip in the incoming twin; (4) by slip in the barrier twin and detwinning of the incoming twin.

In plastic deformation of hexagonal close-packed (hcp) metals, multiple twinning modes [9] can be activated. For Mg, the common twinning modes are $\{10\bar{1}2\}$ extension twinning and $\{10\bar{1}1\}$ contraction twinning, which accommodate the plastic tensile strain and compressive strain along the c-axis, respectively. A $\{10\bar{1}2\}$ twin can consume a whole grain under favorable loading condition [10]. Therefore, considerable twin-twin interactions can occur in a single grain when multiple twin variants exist. In the literature, the interactions

https://doi.org/10.1016/j.jma.2024.01.032

2213-9567/© 2024 Chongqing University. Publishing services provided by Elsevier B.V. on behalf of KeAi Communications Co. Ltd. This is an open access article under the CC BY-NC-ND license (http://creativecommons.org/licenses/by-nc-nd/4.0/) Peer review under responsibility of Chongqing University

^{*} Corresponding authors.

2

between $\{10\bar{1}2\}$ twin variants can be classified into two types: co-zone twin-twin interaction [11–13], i.e., the interacting twin variants share the same zone axis with the parent, and non-co-zone interaction between variants that share different zone axes with the parent [14–16]. Sun et al. [17] observed that an incoming $\{10\bar{1}2\}$ twin variant can penetrate into the barrier twin variant using high resolution transmission electron microscopy (TEM). Chen et al. [18] reported that highly irregular $60^{\circ}\langle01\bar{1}0\rangle$ boundaries were formed by interaction between non-co-zone twin variants at relatively high strain levels. The atomistic simulation also showed that these boundaries had limited mobility [18].

{1011} twins are typically observed when a compressive load is applied along the c-axis, or a tensile load is applied perpendicular to the c-axis of an HCP crystal with an axial ratio $\gamma = c/a$ less than $\sqrt{3}$ [19]. Thus, they are oftentimes called contraction twinning. It has been experimentally observed that multiple {1011} twin variants can be activated and interact in a single grain in experiments [20–25]. Lin et al. [20] reported that high density {1011} twins were activated and interacted in grains when the tensile load was applied along the (1010) direction of the columnar grains of a Mg alloy. These $\{10\overline{1}1\}$ twins were activated during the plastic deformation up to the fracture strain. Singh et al. [23] also observed that the networks of {1011} twins could cause localized deformation and act as crack initiation sites and propagation paths in bending. Given the significance of this twinning mode in plastic deformation of Mg, especially in strain localization and crack initiation, numerous studies have been performed to elucidate the twin boundary structure and twinning mechanism by high resolution electron microscopy (TEM) [26] and atomistic simulations [27,28]. Similar to the interactions between $\{10\overline{1}2\}$ twin variants [14,18], a $\{10\overline{1}1\}$ twin may interact with its co-zone variant or non-co-zone variant. Recently, Li et al. [24] characterized $\{10\overline{1}1\}$ twins near a fracture surface in an AZ31 Mg alloy by using TEM. Interestingly, an unusual "twin crossing" was captured in which a large {1011} twin variant was able to cross a relatively thin {1011} twin variant. Such a crossing indicates that the twinning dislocations of a $\{10\overline{1}1\}$ twin variant are able to glide into the other variant and transform the lattice of the barrier twin into the lattice of the incoming twin. Crystallographically, such a crossing cannot occur because a twinning dislocation can only glide on the twinning plane which is the first invariant plane. The mechanism for such an unusual interaction between {1011} twin variants has not been understood. Peng et al. [29] also observed crossing of co-zone {1011} twin variants in pure Mg by using TEM and atomistic simulations. They revealed two types of twin-twin interaction: (1) tip-twin penetration in which the tip of a variant could penetrate into its co-zone twin variant; (2) tip-tip collision in which two co-zone twin variants collide and result in the suppression of twin growth. It was also observed that such twin-twin interaction generated high density basal stacking faults inside the twins as well as steps at the twin-twin boundary which was along the $\{10\bar{1}3\}.$

{1011} twins are usually activated at stress levels close to failure of Mg specimens in mechanical testing, and they are associated to crack nucleation [30]. Thus, it is crucial to understand interaction between {1011} twin variants. The purpose of this work is to investigate the interaction between two non-co-zone {1011} twin variants with atomistic simulations. Very interesting interaction behavior is observed, and the mechanism responsible for the interaction is resolved with clarity. The results provide new insight on the mechanism of twin-twin interaction in Mg.

2. Simulation method

There are several Mg potentials reported in the literature, including embedded atom method (EAM) potentials [31,32] developed by Liu et al. [33] and Sun et al. [34], as well as the modified embedded atom method (MEAM) potentials [35] developed by Kim et al. [36] and Wu et al. [37]. These potentials well predict the basal slip and common deformation twinning modes. In addition, the MEAM potentials [36,37] have better capability to describe the $\langle c + a \rangle$ slip. In this work, we aim to investigate the interaction between {1011} twin variants. Thus, the Liu's EAM [33] of low cost and high fidelity is used, which has been used in numerous atomistic simulations of deformation behavior in Mg relating the basal and prismatic slip and deformation twinning [38–40]. The initial perfect Mg single crystal for simulating the interaction between $\{10\overline{1}1\}$ twin variants has dimensions of 25.5 \times 16.5 \times 15.5 nm³ (Fig. 1a), containing a total number of 288,000 atoms. The simulation system is fully relaxed by conjugate gradient energy minimization followed by dynamic relaxation for 60,000 timesteps. The timestep size is 1.0 femtoseconds. After the system is relaxed, a tensile strain is applied along the [2110] direction by moving the left free surface at a constant displacement rate while the right surface is fixed, and the corresponding strain rate is about 4.2×10^9 /sec. The temperature is maintained at 100 K during simulation by using the Nosé-Hoover thermostat [41,42]. Free surfaces are applied to all three dimensions. The simulation results are analyzed by using the non-commercial package Ovito [43]. Simulation package LAMMPS [44] is used for the simulations and calculations in this work. Common neighbor analysis (CNA) [45] is utilized to distinguish the crystal structures and lattice defects.

In our simulations, no pre-existing twins are artificially inserted inside the system. Under the tensile strain perpendicular to the c-axis of the single crystal, $\{10\bar{1}1\}$ twin variants are generated solely by straining.

3. Results

The initial orientation of the Mg single crystal and the loading direction are shown in Fig. 1a. Under the tensile strain perpendicular to the c-axis of the crystal, prismatic dislocations are first nucleated because of finite Schmid factor (\sim 0.43), followed by the nucleation of a $\{10\overline{1}1\}$ twin

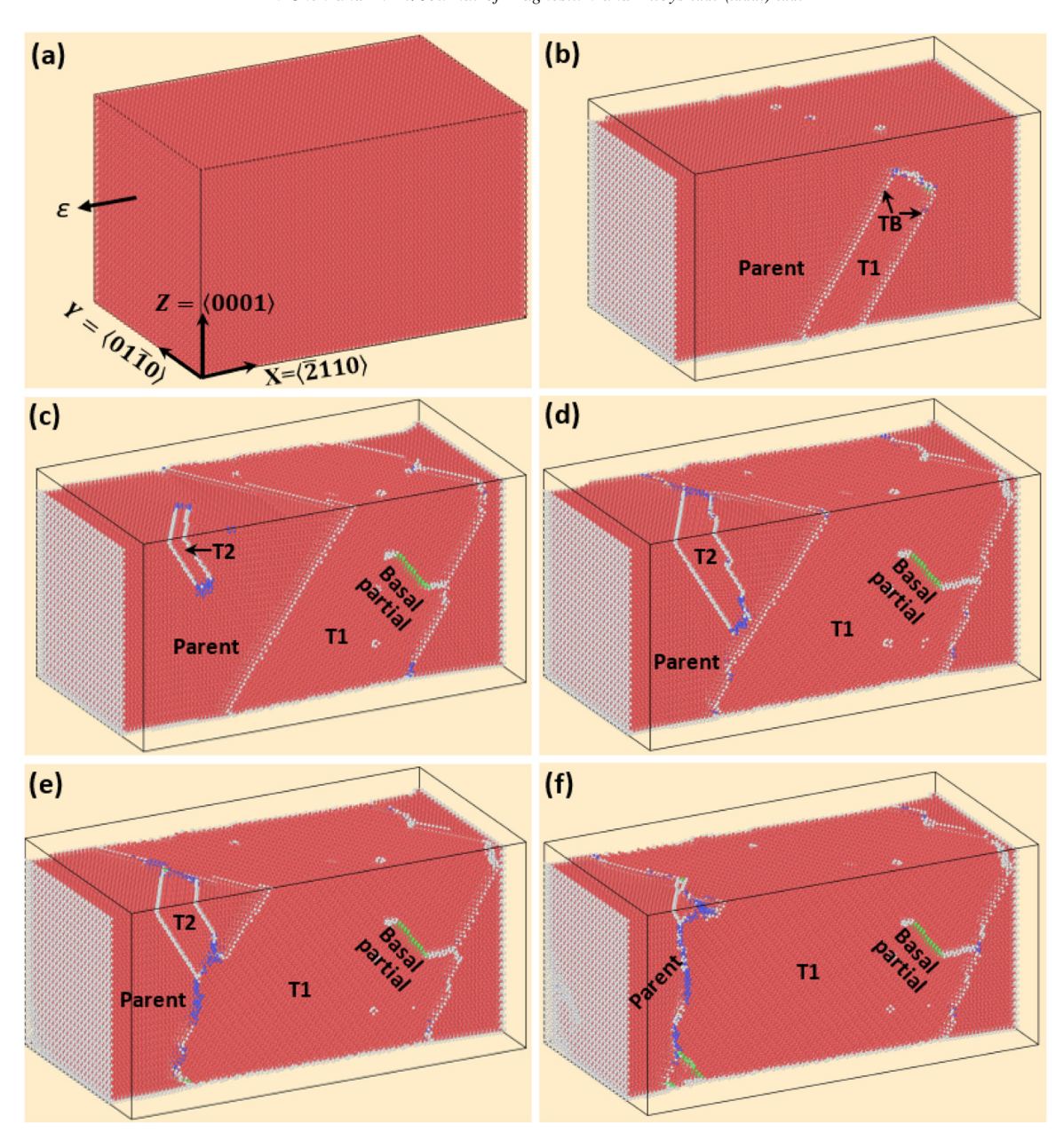


Fig. 1. Snapshots in time sequence showing the interaction between two different $\{10\overline{1}1\}$ twin variants in magnesium in time sequence. (a) A tensile load is applied along the $[2\overline{1}\overline{1}0]$ direction of the simulation box, which favors the $\{10\overline{1}1\}$ twinning but disfavors the basal slip and $\{10\overline{1}2\}$ twinning. (b) A twin variant T1 is activated and grows inside the parent. (c) As the tensile strain is increased, a second twin variant T2 is nucleated. (d) Variant T2 impinges on variant T1. (e) Variant T1 is growing at the expense of variant T2. (f) Variant T2 is almost consumed by variant T1.

(labeled as T1). T1 is nucleated from the bottom free surface and grows upward into the crystal (Fig. 1b). As the tensile strain increases, T1 thickens while its twin tip reaches the top free surface (Fig. 1c). Details of how twinning dislocations mediating twin growth will be analyzed below. Meanwhile, a second {1011} twin variant is nucleated at the top surface and the twin tips are growing toward one of the twin boundaries (TBs) of T1. The green atoms inside T1 corresponds to a basal stacking fault (SF). Such basal SFs are commonly observed inside {1011} and {1012} deformation twins as a result of large atomic shuffles that are required for atoms in parent lattice to reach the twin positions and the formation

of these SFs has nothing to do with glide of Shockley partial dislocations [46–51]. These SFs are called "partial stacking faults" because only those atoms on every other basal plane are displaced by the formation of SFs [46–48,50].

As the tensile strain further increases, T2 thickens by nucleation of more twinning dislocations and eventually the twin tip impinges on the TB between T1 and the parent (Fig. 1d). Very interestingly, the impingement of the twin tip of T2 does not hinder the growth of T1 as the external strain continues increasing (Fig. 1e). Instead, T1 further thickens at the expense of T2 and the parent. At the end of the simulation, T2 is almost consumed by T1 (Fig. 1f). This indicates that the

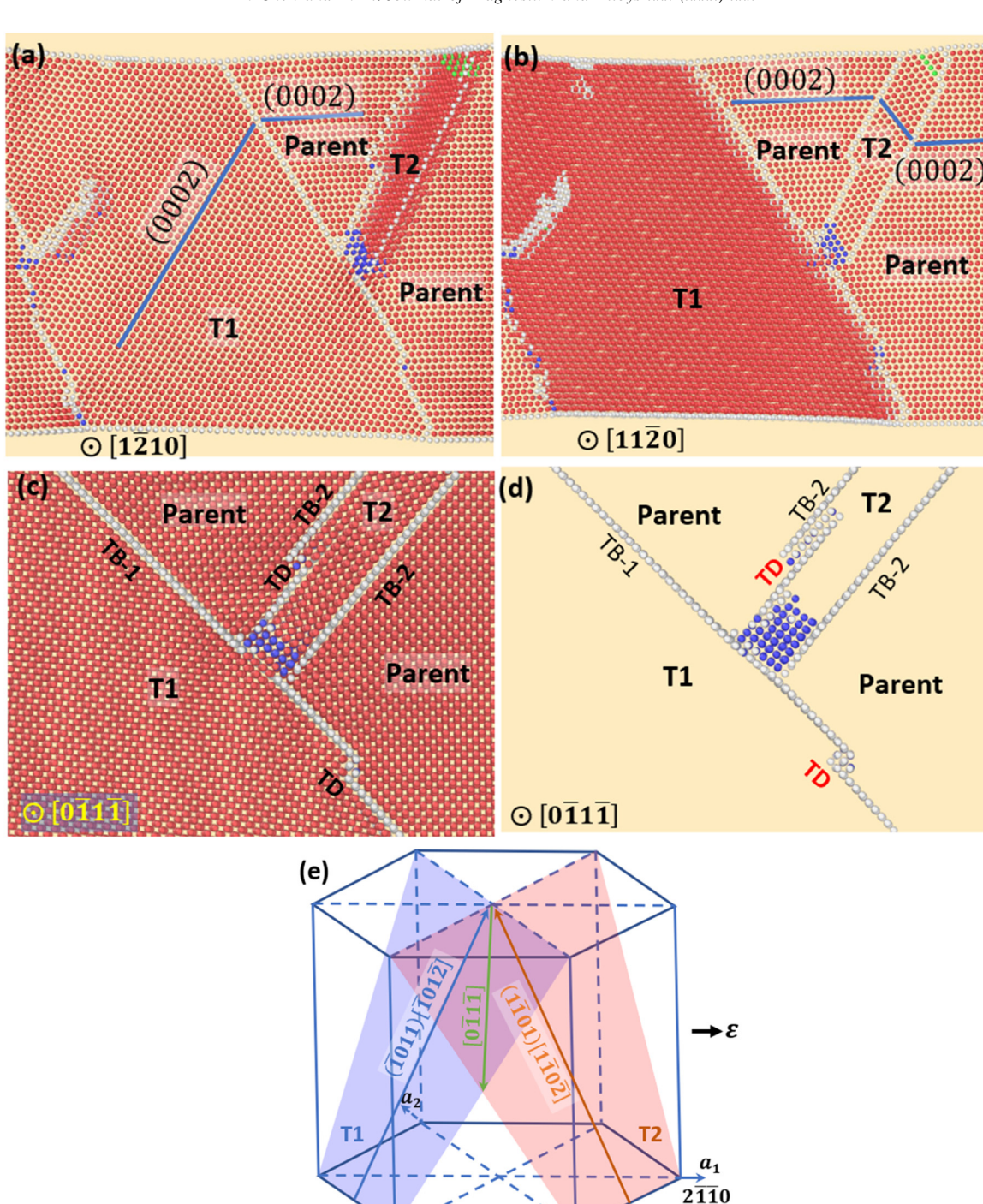


Fig. 2. Orientation relationship between variant T1 and T2. (a) The lattice is tilted such that the zone axis of T1 and parent is along the viewing direction, i.e., $[1\bar{2}10]$. This twin variant T1 satisfies $56^{\circ}[1\bar{2}10]$ relationship with respect to the parent, thus it is a $(\bar{1}011)$ variant. (b) The zone axis of variant T2 and parent is identified as $[11\bar{2}0]$, indicating T2 is a $(1\bar{1}01)$ variant. (c) Edge-on view along the zone axis of variant T1 and T2, i.e. $[0\bar{1}1\bar{1}]$. (d) The atoms in perfect hcp lattice are hidden, the twin boundaries (in white) are all edge-on. (e) Crystallography of variant T1 and variant T2. The intersection line (zone axis of variant T1 and T2) is along the $[0\bar{1}1\bar{1}]$. The twinning dislocations are all two-layer zonal dislocations.

twinning dislocations for T1 can also glide on the interface between T1 and T2 and pass through the T2 lattice.

4

To determine the twin orientation relationship of T1 and T2, the system is carefully tilted to various viewing directions such that the TBs can be well resolved. In Fig. 2a, the sim-

ulation system is tilted such that the zone axis between T1 and the parent is along the viewing direction, i.e., $[1\bar{2}10]$. In this viewing direction, the basal plane of the parent and T1 and the TB between T1 and the parent are all edge-on. The atoms in perfect hcp lattice are shown in red in the common

neighbor analysis. The basal planes of the parent and T1 are denoted by the blue lines. It can be seen that T1 satisfies $56^{\circ}[1\bar{2}10]$ relationship with respect to the parent, and the TB is exactly along the $(\bar{1}011)$ plane of the parent. Thus, T1 is indeed a $(\bar{1}011)$ variant. When the system is tilted such that the basal plane of T2 and the parent and the TB between T2 and the parent are all edge-on (Fig. 2b), it can be seen that T2 is a $(1\bar{1}01)$ variant. The zone axis between T2 and the parent is $[11\bar{2}0]$. Obviously, T1 and T2 are not co-zone twin variants.

After the $\{10\overline{1}1\}$ twin variants are properly identified, the system is tilted such that both lattice of T1 and T2 can be well resolved. The viewing direction is thus along the zone axis of T1 and T2. In this viewing direction, i.e., [0111], the twinning planes of T1 and T2 can be viewed edge-on simultaneously, and the twin-twin interaction can be clearly resolved (Fig. 2c). Those atoms at the twin-twin interaction region are displayed in blue. It can clearly be seen that two-layer steps are present at the interface between T1 and the parent (this interface is denoted as TB-1), and at the interface between T2 and the parent (these interfaces are denoted as TB-2). These steps are the core of two-layer zonal twinning dislocations that mediate the growth of the {1011} twin variants (see Fig. 3 below). After we hide those red atoms on the perfect HCP positions, only the TBs, the twin-twin interaction region, and the zonal twinning dislocations are revealed (Fig. 2d). The crystallographic relationship between T1, T2 and the parent is displayed in Fig. 2e. The blue and brown shaded planes are the $(\bar{1}011)$ and the $(1\bar{1}01)$, which are the twinning planes for T1 and T2, respectively. These two twinning planes intersect at the green line which is along the $[0\bar{1}1\bar{1}]$, i.e., the zone axis of the two twin lattices.

To show the twinning dislocation lines that are gliding on TB-1, we make projection views that are along the plane normal of TB-1 (Fig. 3). As the tip of T2 impinges on TB-1, a twinning dislocation is nucleated at the impingement (Fig. 3a). This twinning dislocation is gliding on TB-1 and thickening T1 at the expense of both the parent and T2. As this twinning dislocation keeps gliding away, another twinning dislocation is nucleated also at the impingement (Fig. 3c-d). Thus, the twin-twin interaction facilitates nucleation of twinning dislocations that thicken T1, but consume T2.

4. Analysis and discussion

4.1. Unusual transmutation of zonal twinning dislocations during twin-twin interaction

The atomistic simulation results in this work reveal an interesting twin-twin interaction between two non-co-zone {1011} variants. It appears that the twinning dislocation of one variant is able to pass through the other during twin-twin interaction. As a result, a variant grows at the expense of the other. Such a twin-twin interaction is quite unusual for dislocation-mediated twinning modes. According to the pioneering works by Bilby and Crocker [52], Christian and

Mahajan [7], the twinning dislocation of $\{10\overline{1}1\}\langle10\overline{12}\rangle$ mode is a four-layer zonal twinning dislocation, indicating that the twinning dislocation should comprise four {1011} twinning planes simultaneously. This is because the K₂ plane, i.e., the second invariant plane, intersects every fourth K₁ plane, i.e., the first invariant plane, at a lattice point. The atoms at these intersecting points are directly sheared to the twin positions by the zonal twinning dislocation without atomic shuffles, but shuffles must be involved for the other atoms because a homogeneous shear alone cannot carry these atoms to the twin positions. Li and Ma [27] showed that a four-layer zonal twinning dislocation tends to dissociate into two double-layer partial zonal twinning dislocations, as observed in Fig. 2cd. Thus, the Burgers vector of a zonal twinning dislocation is strictly defined by the crystallographic relationship between the parent and the twin lattice, and should remain on the twin boundary which is the interface between the parent and twin. Theoretically, the twinning dislocation of one variant cannot pass through the other and twin growth would stop due to the twin-twin interaction. The fact that T1 consumes T2 via the glide of twinning dislocations through the lattice of T2 indicates that a very special process of twin-twin interaction has occurred. To resolve this mechanism, we carefully analyze the interaction process as follows.

Our analyses are focused on the region where the twin variants intersect. To pinpoint this region, we first take out a small volume of atoms that contains the parent, T1 and T2, as shown in Fig. 4a. The TBs are colored in white according to CAN [45]. Then the atoms on the perfect HCP positions are hidden out and only those atoms on TB-1 and TB-2 can be seen (Fig. 4b). Four snapshots in time sequence showing the evolution at the TBs during twin-twin interaction are displayed in Fig. 4c-d. The selected region is slightly tilted such that all the TBs are close to edge-on. In Fig. 4c, T2, which is much thinner than T1, is approaching T1. Eventually, the tip of T2 impinges on T1 (Fig. 4d). After the impingement, the twinning dislocations on TB-2 stop gliding and are unable to penetrate into T1. Thus, the lengthening of T2 is stopped by the twin-twin interaction. Shortly after T2 impinges on T1, a double-layer twinning dislocation loop is nucleated at the location of impingement, and this twinning dislocation is gliding on TB-1 with a Burgers vector of $\frac{4\gamma^2-9}{2(4\gamma^2+3)}[\bar{1}01\bar{2}]_{T1}$ (where γ is the c/a ratio, 1.624 for Mg) (Fig. 4e). This twinning dislocation loop thickens T1 by two atomic layers as the loop expands on TB-1 (Fig. 4f). Note that the snapshots are only a thin slice of the simulation system, so the dislocation loop is truncated and appears to be two separate segments that are gliding on TB-1.

The above process repeats as the tensile strain increases. More twinning dislocations are nucleated on TB-1 and TB-2 that thicken both variants. However, the twinning dislocations on TB-2 are blocked by T1 at the interface of twin-twin interaction. Fig. 5a shows that another twinning dislocation with a Burgers vector of $\frac{4\gamma^2-9}{2(4\gamma^2+3)}\langle 1\bar{1}0\bar{2}\rangle_{T2}$ is gliding on TB-2 toward T1. Eventually this twinning dislocation impinges on the T1-T2 interface and its glide is stopped. The impinge-



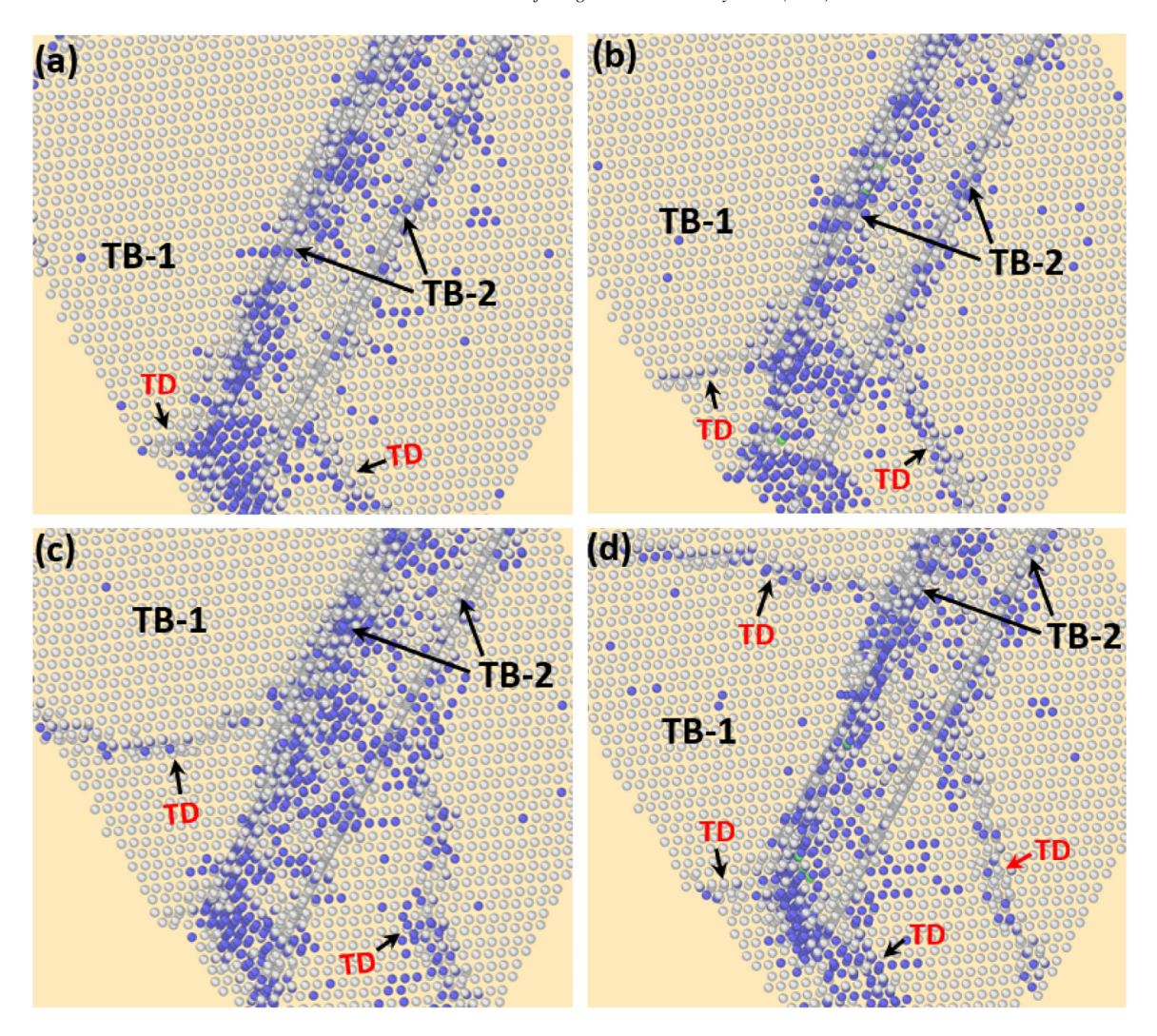


Fig. 3. (a) Projection view of {1011} twin-twin interaction. The viewing direction is along the normal of TB-1 which is the interface between variant T1 and the parent. The TB-2 s between variant T2 and the parent are indicated by the black arrows. TB-2 s are intersecting TB-1. It can be better seen that TDs (indicated by the black arrows) on TB-1 are nucleated at the intersection of the two variants. (b) The TDs on TB-1 glides and consumes the parent and grows variant T1. (c) and (d) More TDs are nucleated at the twin-twin intersection which grows variant T1 at the expense of the parent and variant T2.

ment causes nucleation of a twinning dislocation on TB-1 that thickens T1 (Fig. 5b-d). To better reveal the structure of the double-layer zonal twinning dislocations, we slightly tilt the system such that the dislocation lines can be better seen (Fig. 6a-d). It is clearly seen that the double-layer twinning dislocation is nucleated at the twin-twin interaction on TB-1 and then glide and thickens T1, meanwhile, the length of T2 is reduced by two layers. Although the length of T2 is reduced by the growth of T1, T2 keeps thickening by nucleating more twinning dislocations on TB-2 (Fig. 6c-d). Thus, it appears that the impingement of twinning dislocations for T2 at the twin-twin interaction facilitates nucleation of twinning dislocations for T1 which thickens T1 at the expense of T2.

In addition to nucleation of twinning dislocations for T1 due to twin-twin interaction, twinning dislocations can also be nucleated at the intersection of T1 with the free surfaces. Then these twinning dislocations glide toward the twin-twin

intersection. Fig. 7a shows that a double-layer twinning dislocation on TB-1 is nucleated at the free surface and gliding toward the intersection between T1 and T2. Interestingly, this twinning dislocation, which glides on TB-1, is able to readily pass through the lattice of T2 (Fig. 7b-c). As a result, the length of T2 is reduced by two layers as the twinning dislocation on TB-1 glides away (Fig. 7d). In Fig. 7a-d, there is another twinning dislocation on TB-2 which is also gliding toward the intersection of the twin variants. This twinning dislocation is unable to glide down and impinge on TB-1 until the twinning dislocation on TB-1 glides away, due to the repulsive force between the two twinning dislocations.

Recently, Alkan et al. [6] investigated twin-twin interaction in a face-centered-cubic (FCC) high entropy alloy (HEA), and showed that when the twinning dislocation of an incoming twin interacted with the TB of a barrier twin, a residual dislocation and a twinning partial were created. This newly created twinning partial mediated the migration of the twin

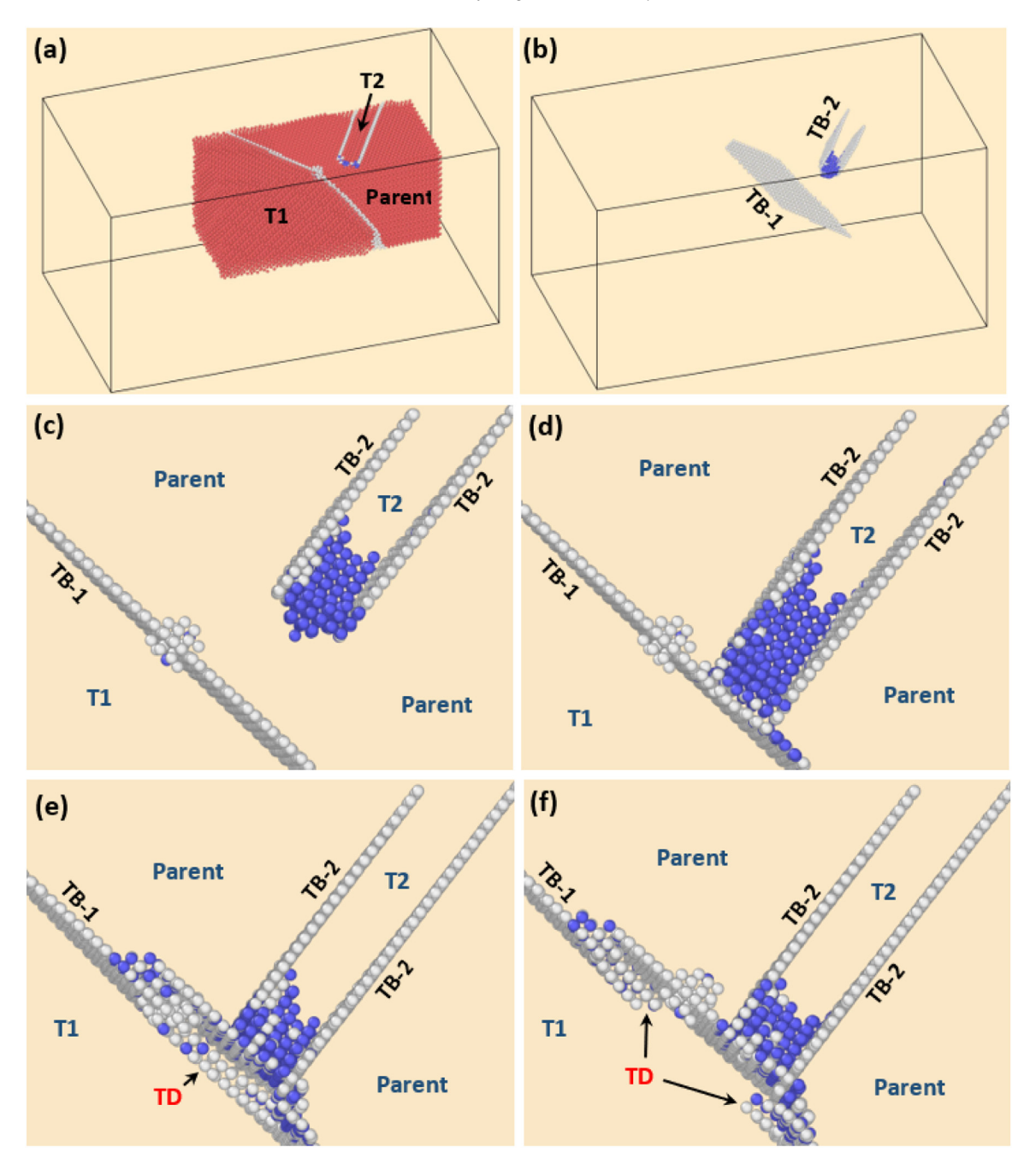
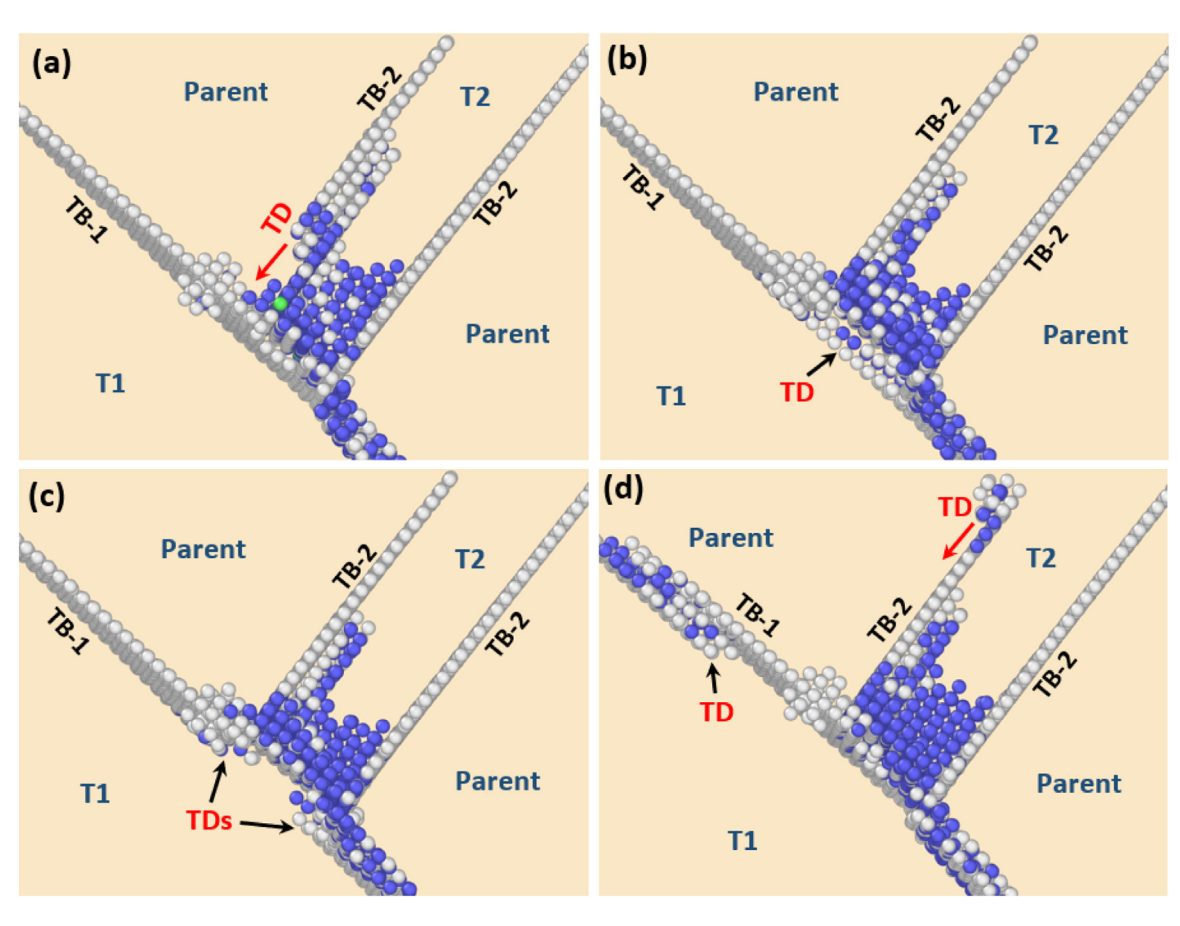


Fig. 4. Structural evolution at the twin TBs when variant T2 impinges on variant T1. (a) A portion of the system that contains the parent, T1 and T2 is selected to better reveal the twin-twin interaction. (b) The atoms in the perfect hcp lattice of (a) are hidden, and only the TBs are shown. (c) A magnified view where variant T2 is growing toward variant T1. The TB between T1 and the parent is denoted as TB-1 whereas the TBs between T2 and the parent is denoted as TB-2. (d) Variant T2 impinges on variant T1. (e) During twin-twin interaction, a two-layer zonal TD (denoted by the black arrow) nucleates at the intersection. (f) This TD glides on TB-1 and thickens variant T1 by two atomic layers. Note that part of variant T2 at the intersection is consumed and transformed into variant T1 by the TD.

boundary of barrier twin. Similarly, for $\{11\overline{2}2\}$ twin-twin interaction in HCP titanium, Sui et al. [53] proposed that when an incoming twin variant impinged on a barrier twin variant, the incoming twinning dislocation could dissociate at the intersection and generate a twinning dislocation which resulted in detwinning of the barrier twin. Additionally, an $\langle a \rangle$ dislocation was released into the barrier twin. This proposition is

similar to Rémy's analysis [8] that the localized shear at the twin-twin intersection was mitigated by emitting a dislocation slip in barrier twin.

If a similar twinning dislocation reaction also happens to the $\{10\bar{1}1\}$ twin-twin interaction in our simulation, i.e., the incoming twinning dislocation for T2 dissociates at the twin-twin intersection and produces a twinning dislocation for T1



P. Chen and B. Li/Journal of Magnesium and Alloys xxx (xxxx) xxx

Fig. 5. (a) A zonal TD of variant T2 is gliding on TB-2 towards variant T1. (b) The zonal TD on TB-2 impinges on TB-1. Meanwhile, a TD of variant T1 is nucleated at the intersection and glides on TB-1. (c) The TD on TB-1 glides and thickens variant T1. (d) As the TD on TB-1 thickens variant T1, it transforms part of variant T2 into variant T1.

and a residual dislocation, then the dislocation reaction would be written as follows:

$$\frac{4\gamma^{2}-9}{2(4\gamma^{2}+3)}\langle 1\bar{1}0\bar{2}\rangle_{T2} \rightarrow \frac{4\gamma^{2}-9}{2(4\gamma^{2}+3)}\langle \bar{1}01\bar{2}\rangle_{T1} + \frac{4\gamma^{2}-9}{2(4\gamma^{2}+3)}\langle 2\bar{1}\bar{1}0\rangle_{Residual} \quad (1)$$

According to Frank's rule which requires the angle between the two partial dislocations be greater than 90° [54] such that the total elastic energy of the dislocations decreases after dissociation, such a dissociation is energetically unfavorable. It should be noted that Frank's rule only applies to dissociation of lattice dislocations. For interfacial dislocations such as twinning dislocations that glide on a twin boundary, such dissociation might still occur, just like the creation of accommodative dislocations at a twin tip by dissociation of a twinning dislocation in body-centered-cubic metals [55]. From our simulation results, no residual dislocation emission is observed either in T1 (the barrier twin) or in T2 (the incoming twin) (Fig. 4-7). Therefore, it is more likely that the nucleation of twinning dislocation of T1 is facilitated by the local stress at the intersection due to the twinning dislocations on TB-2.

Twin-twin interaction mechanism is also dependent on dislocation density. Lv et al. [5] observed complex twin-twin interaction in a FCC nickel based superalloy. They found that tangled matrix dislocations near a barrier twin effectively blocked the growth of an incoming twin; in some cases, an incoming twin seemed to penetrate a barrier twin. But exactly how the incoming twin penetrated the barrier twin was not explained. In our work, the thick T1 is able to consume the thin T2. Thus, the thickness of the twin variants may also affect the form of twin-twin interaction. Presumably, the twinning dislocations of the thick variant would penetrate the thin variant more favorably, whereas it would be harder for the twinning dislocations of the thin variant to pass through the thick variant.

4.2. Lattice transformation analysis during interaction of {1011} variants

The results in Fig. 4-7 show that the twinning dislocation of T1 is able to transform the lattice of T2 into the lattice of T1. However, the lattice transformation mechanism for $T2 \rightarrow T1$ must be different from that for parent $\rightarrow T1$. Thus, for some reason, these two different lattice transformation processes generate the same product lattice of T1, which is unusual. Christian stated that during deformation twinning and solid state phase transformations, there exists a one-toone lattice correspondence between the parent lattice and the product lattice [56]. This fundamental principle implies that atoms on a crystallographic plane of the parent lattice will

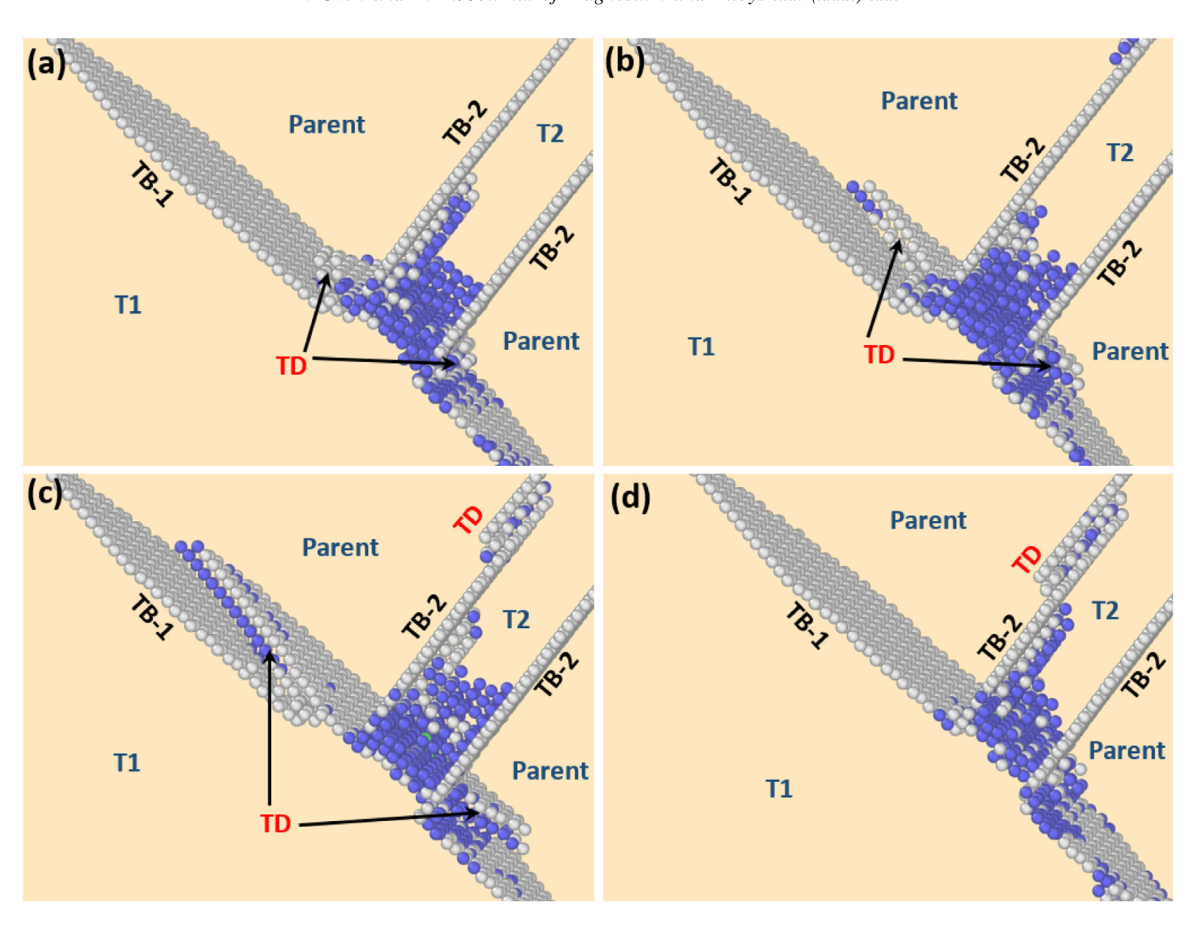


Fig. 6. Tilted views of the structure of the TBs during $\{10\overline{1}1\}$ twin-twin interaction. (a) The intersection of $\{10\overline{1}1\}$ twin variants becomes a source for nucleating TDs that grows variant T1 at the expense of the parent and variant T2. (b) The morphology of TDs is clearly a two-layer zonal dislocation. (c) The TDs glide on TB-1. (d) The TDs glide out to the surface and variant T1 is thickened by two atomic layers. Meanwhile, a TD on TB-2 is nucleated and grows variant T2.

be located on the corresponding plane of the product lattice after twinning or phase transformation is completed. Basinski et al. used lattice correspondence to explain hardness increase in deformation twins as a result of mobile lattice dislocations becoming immobile after twinning [57]. Because the twinning elements are well defined crystallographically, lattice correspondences in twinning modes can be calculated mathematically. Niewczas calculated the corresponding planes in all four major twinning modes in HCP metals [58] and the results for $\{10\overline{1}2\}\langle10\overline{1}\overline{1}\rangle$ mode show that the parent basal plane is transformed into the twin prismatic plane, and the parent prismatic plane is transformed into the twin basal plane. This lattice correspondence is consistent with numerous atomistic simulations [46,51,59,60]. Chen et al. investigated twin-slip interaction in Mg and found that the interaction well follows the principle of lattice correspondence [38,61].

The crystallographic analysis for parent \rightarrow T2 \rightarrow T1 lattice transformations is displayed in Fig. 8. To conduct this analysis, we first select and take out seventeen atoms of an HCP unit cell of variant T2. Then we track the evolution of the positions of these atoms throughout the simulation. To better reveal how the selected unit cell transforms sequentially, the seven atoms on the top basal plane are colored in

blue, the three atoms on the middle basal plane in green, and the seven atoms on the bottom basal plane in red. To help identify the corresponding planes, the HCP unit cells are delineated and some atomic planes are shaded to highlight their transformations. First, we examine how the parent lattice is transformed into the T2 twin lattice. We play the simulation backward from T2 to a timestep when the selected atoms are in the parent lattice. It can clearly be seen that the seven blue atoms on the T2 basal plane now reside on the {1011} plane (highlighted in yellow) of the parent; whereas the atoms on the {1011} plane of T2 (highlighted in light blue) now reside on the basal plane of the parent. Note that the $\{10\overline{1}1\}$ plane is a corrugated plane, i.e., the atoms on this plane reside on two slightly separated atomic layers. This can be seen from the highlighted {1011} plane of T2, where the two green atoms are not on the same plane containing the three red atoms and the two blue atoms. Before twinning, these atoms are located on the basal plane of the parent which is single-layered. Therefore, atomic shuffling must be involved for {1011} twinning mode. The lattice correspondence for parent \rightarrow T2 transformation can be described as:

$$\{10\bar{1}\bar{1}\}_{parent} \to (0002)_{T2} \text{ and } (0002)_{parent} \to \{10\bar{1}\bar{1}\}_{T2}$$



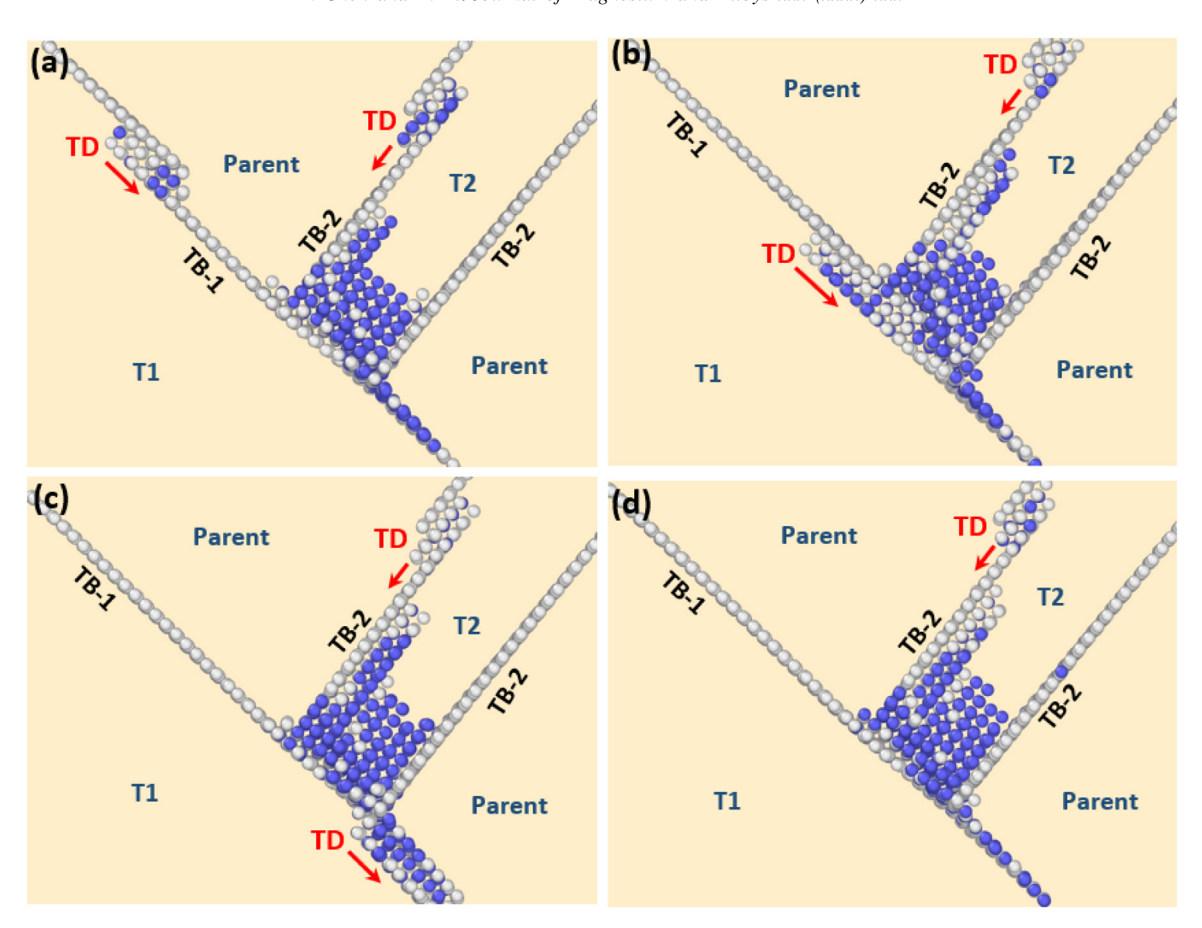


Fig. 7. (a) A zonal TD on TB-1 can also be nucleated at the intersection of variant T1 and the free surface, and then glides toward the twin-twin intersection. (b) The TD on TB-1 approaches the twin-twin intersection. (c) The TD on TB-1 is able to pass through the twin-twin intersection. (d) The TD on TB-1 consumes a thin layer of variant T2 and transforms it into variant T1.

This lattice transformation is consistent with the crystallography-based calculation by Niewczas [58].

Next, we play the simulation forward. After the twinning dislocations on TB-1 pass through the T1-T2 intersection, the selected seventeen atoms are now located in the T1 lattice. It can be seen that, the seven red atoms on the T2 basal plane now reside on one of the prismatic planes of the T1 lattice. Similarly, the seven blue atoms on T2 basal plane also reside on the prismatic plane of the T1 lattice. Moreover, the prismatic planes of T2 (hatched with blue lines) are transformed into the basal planes of T1. The middle prismatic plane of T2 that comprises three blue atoms connected by the blue line on the top basal plane and the three red atoms connected by a blue line on the bottom basal plane, as well as two green atoms of the middle basal plane is transformed into the middle basal plane of T1. So, the lattice correspondence of T2 \rightarrow T1 transformation can be described as:

$$(0002)_{T2} \rightarrow \{10\overline{1}0\}_{T1} \text{ and } \{10\overline{1}0\}_{T2} \rightarrow (0002)_{T1}$$

Immediately, it can be seen that the $T2 \rightarrow T1$ lattice transformation is exactly the same as the lattice transformation of $\{10\bar{1}2\}\langle10\bar{1}\bar{1}\rangle$ twinning mode in HCP metals including Mg. This twinning is the most commonly observed mode in HCP metals. For Mg, the critical stress for activating this twinning

mode is on the order of a few MPa [62]. Thus, somehow the $T2 \rightarrow T1$ transformation is very close to $\{10\bar{1}2\}\langle10\bar{1}\bar{1}\rangle$ twinning, but the orientation relationship is not exactly the same, as seen in the following analyses.

To reveal the orientation relationship between T1 and T2 twin variant, we carefully tilt the T2 lattice comprising the selected atoms to two special viewing directions, i.e., [0002] and [1010]. In these viewing directions, the lattice transformation can be better resolved. Fig. 9a shows the HCP unit cell in T2 when viewed along the [0002] direction. The blue, green and red atoms are on three consecutive basal planes (the red atoms are right behind the green and blue atoms). After the twinning dislocations of T1 pass through the twin-twin intersection, these atoms now reside on the lattice of T1 (Fig. 9a). Several key features can be seen. The c-axis of T1 and T2 are nearly perpendicular to each other. The [1010] prismatic plane of T2, which has a double-layered structure that contains a layer of green atoms and a mixed layer of blue and red atoms, has been transformed into the single-layered basal plane of T1 where the blue, green and red atoms all reside on a single-layered plane. If we examine the positions of the blue atoms that are on the basal plane of T2, they are now on the prismatic plane of T1. Note that the structure of the prismatic plane of T1 is very close to the structure of the basal

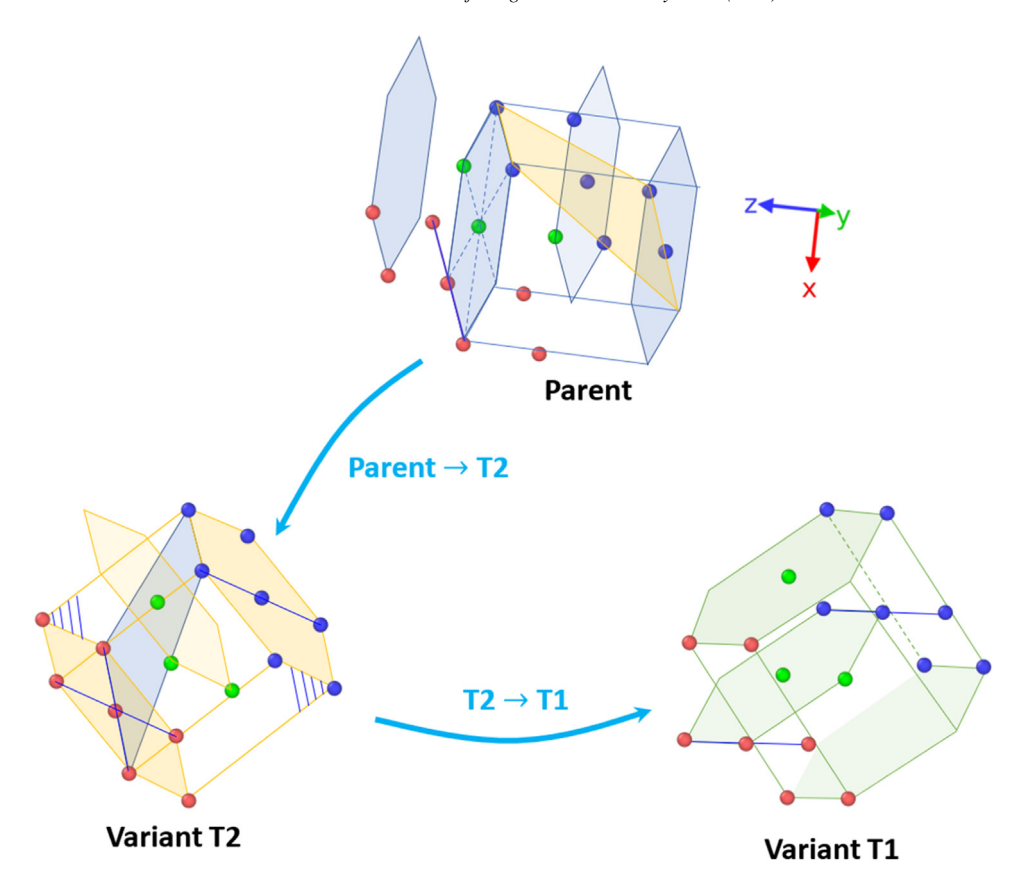


Fig. 8. Analysis of lattice transformations during $\{10\bar{1}1\}$ twin-twin interaction. The initial parent lattice is first transformed to variant T2 which is subsequently transformed to variant T1. A total of seventeen atoms of in variant T2 are first selected. The atoms on three neighboring basal planes are colored in red, green and blue, respectively. The positions of these selected atoms are tracked. Then, the simulation is played backward before the twin variants are formed such that the colored atoms are now in the parent lattice. It can be seen that the lattice transformation from the parent to T2 is such that the (0002) basal plane is transformed into the $\{10\bar{1}1\}$ of T2, and the $\{10\bar{1}1\}$ of parent is transformed into the (0002) basal of T2. When the simulation is played forward such that the colored atoms are now in T1, it can be seen that the *c*-axis of T1 and T2 are nearly perpendicular to each other. The basal plane of T2 is transformed into the prismatic plane of T1, and the prismatic plane of T2 (hatched with blue lines) is transformed into the basal plane of T1. Detailed lattice correspondence from T2 to T1 is analyzed in Fig. 9 and 10.

plane of T2. When viewed along this viewing direction which is close to but not exactly the [1010] direction of T1, the blue atoms of T1 appear to be on a hexagonal plane, but they are not. These blue atoms are actually located on two slightly separated planes that constitute the double-layered structure of the prismatic plane (cf. Fig. 8). Next, we superimpose the T2 lattice with the T1 lattice, but shrink the spheres of individual atoms so that they do not overlap. This way, the paths and displacements how individual atoms of T2 reach T1 can be visualized, as shown by the red arrows in Fig. 9b. The red, green and blue dashed circles represent the positions of atoms in the T1 lattice. Red arrows are drawn from the lattice positions of T2 to those of T1. The maximal magnitude of these atomic shuffles is roughly $\frac{\sqrt{3}}{6}a_0$ ($a_0 = 3.21$ Å is the lattice parameter of pure Mg) along the [1010] such that the double-layered prismatic plane of T2 is transformed into the single-layered basal plane of T1. If we compare the two lattices of T1 and T2 in this viewing direction, a salient feature can be seen. The basal plane of T1 is slightly rotated by \sim 7° relative to the prismatic plane of T2. But for $\{1012\}\langle 1011\rangle$

twinning, this angle should equal zero because the zone axis of this twinning mode is the $\langle 1\bar{2}10 \rangle$ and the twin lattice is reoriented around this zone axis by roughly 90°

Next, we tilt the T2 lattice to the viewing direction along the [$10\bar{1}0$] of T2, as shown in Fig. 10a. Now the front plane is the prismatic plane of T2. After lattice transformation, the originally single-layered blue, green and red basal planes of T2 now become double-layered prismatic planes of T1. However, it can be seen that the T2 lattice is also slightly tilted around this viewing direction, in addition to the \sim 7° tilting observed in Fig. 9. Again, we superimpose the T1 and T2 lattice, as shown in Fig. 10b. The red and blue dashed circles represent the positions of T1. The red arrows pointing from the T2 position to T1 positions indicate the displacements of individual atoms during the lattice transformation from T2 to T1. The tilt angle between the prismatic plane of T1 and the basal plane of T2 is about 7.5°

Fig. 9-10 indicate that the lattice transformation from T2 to T1 is very close to $\{10\overline{1}2\}\langle10\overline{1}\overline{1}\rangle$ twinning, but with an additional tilt that is not seen in the ideal $\{10\overline{1}2\}\langle10\overline{1}\overline{1}\rangle$.

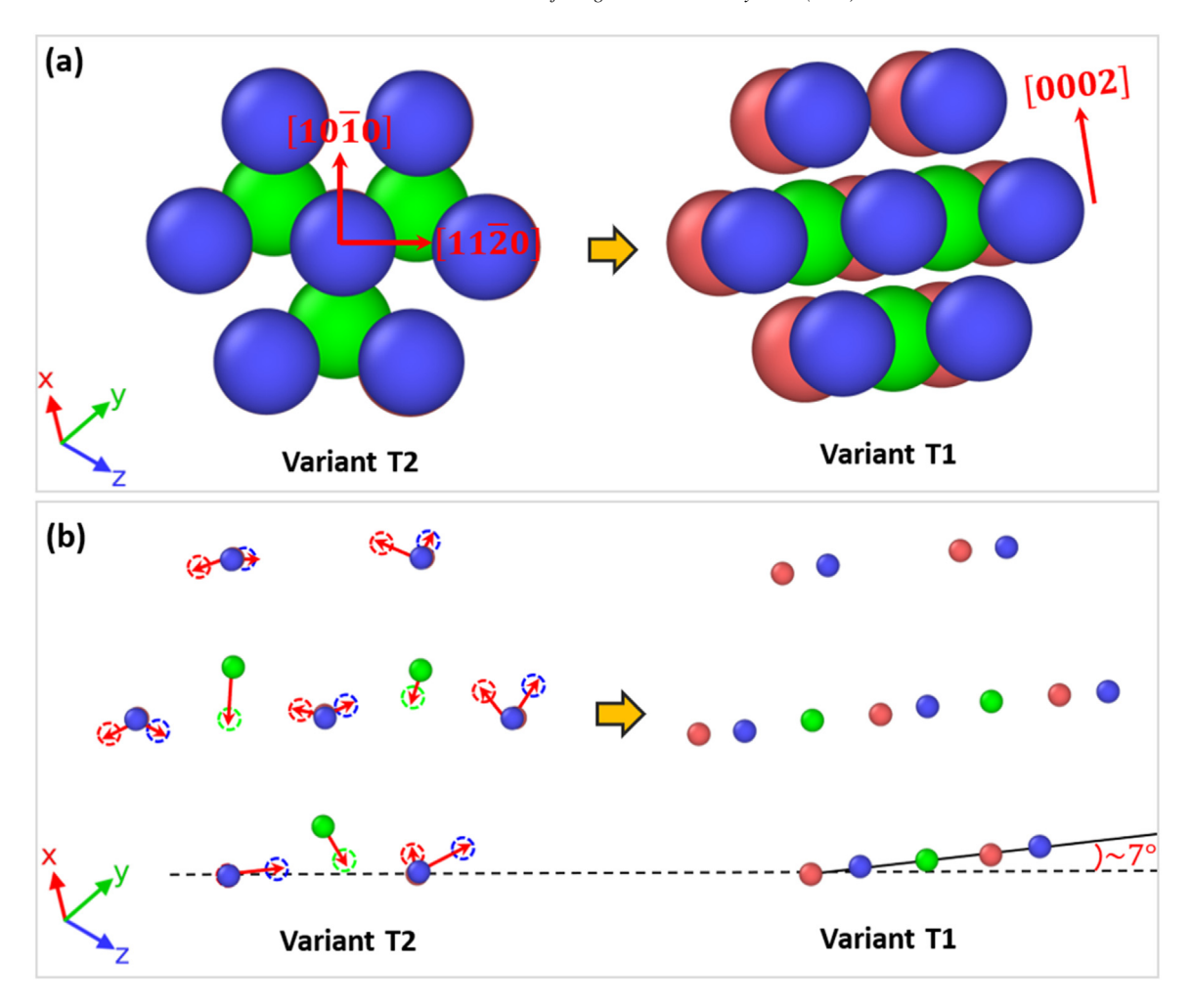


Fig. 9. Lattice transformation analysis between variant T1 and T2 when viewed along the [0002] direction of T2. (a) The pre-selected atoms in variant T2. After lattice transformation, the double-layered prismatic planes of T2 are transformed into the single layer basal planes of variant T1. Note that the blue atoms on the basal of T1 now reside on the prismatic plane of T1, and the T1 lattice is slightly tilted relative to T2. (b) The lattice of T1 and T2 are superimposed. The dashed circles represent the corresponding positions of atoms after lattice transformation. The red arrows indicate the major atomic displacements from T2 to T1. The tilt angle is approximately 7° about the viewing direction. The X-Y-Z axes represent the original coordinate system of the single crystal.

This additional tilt makes the T2 \rightarrow T1 transformation harder than $\{10\bar{1}2\}\langle10\bar{1}\bar{1}\rangle$ twinning and the parent \rightarrow T2, i.e., $\{10\bar{1}1\}\langle10\bar{1}\bar{2}\rangle$ twinning.

4.3. Dislocation-mediated and non-dislocation-mediated twin-twin interaction

The twin-twin interaction between non-co-zone {1011} variants observed in our simulations involves activities of zonal twinning dislocations at the twin boundary and the twinning dislocations of a variant can penetrate the lattice of the other variant. The penetration is accomplished by the co-action of a shear mediated by the twinning dislocations and atomic shuffles. Due to the additional tilt (Fig. 9-10), the atomic shuffles must be different from the shuffles that are required for $\{10\bar{1}1\}\langle10\bar{1}\bar{2}\rangle$ twinning. Thus, the shuffles for the zonal twinning dislocations on TB-1 and TB-2 (Fig. 4-7), i.e., before the twin-twin interaction, and the shuffles during twin-twin interaction must be different. It can be expected that the core structure of the twinning dislocation during twin-twin

interaction should also be different from that before the interaction. Such a difference can be accommodated by the nature of zonal twinning dislocations which typically comprise multiple slip planes simultaneously. The displacement and shuffling direction of individual atoms on each slip plane do not have to be the same and can be quite different [63,64,50]. Thus, when the zonal twinning dislocations on TB-1 are plowing through the twin-twin intersection and transform the T2 lattice into T1, the shuffling mode may vary to accommodate the different atomic environments. The shuffling mode is recovered after the twinning dislocations pass through the twin-twin intersection. However, such a twin-twin interaction is expected to "hard", as shown by the increase in the energy barrier (Fig. 11), and can be characterized as "hard twin-twin interaction".

In contrast to the dislocation mediated twin-twin interaction, non-dislocation-mediated twin-twin interaction has been reported and such an interaction is typically found in $\{10\bar{1}2\}\langle10\bar{1}\bar{1}\rangle$ twinning mode. Note that the $\{10\bar{1}2\}$ twinning mode has been treated as a classical twinning, similar to the

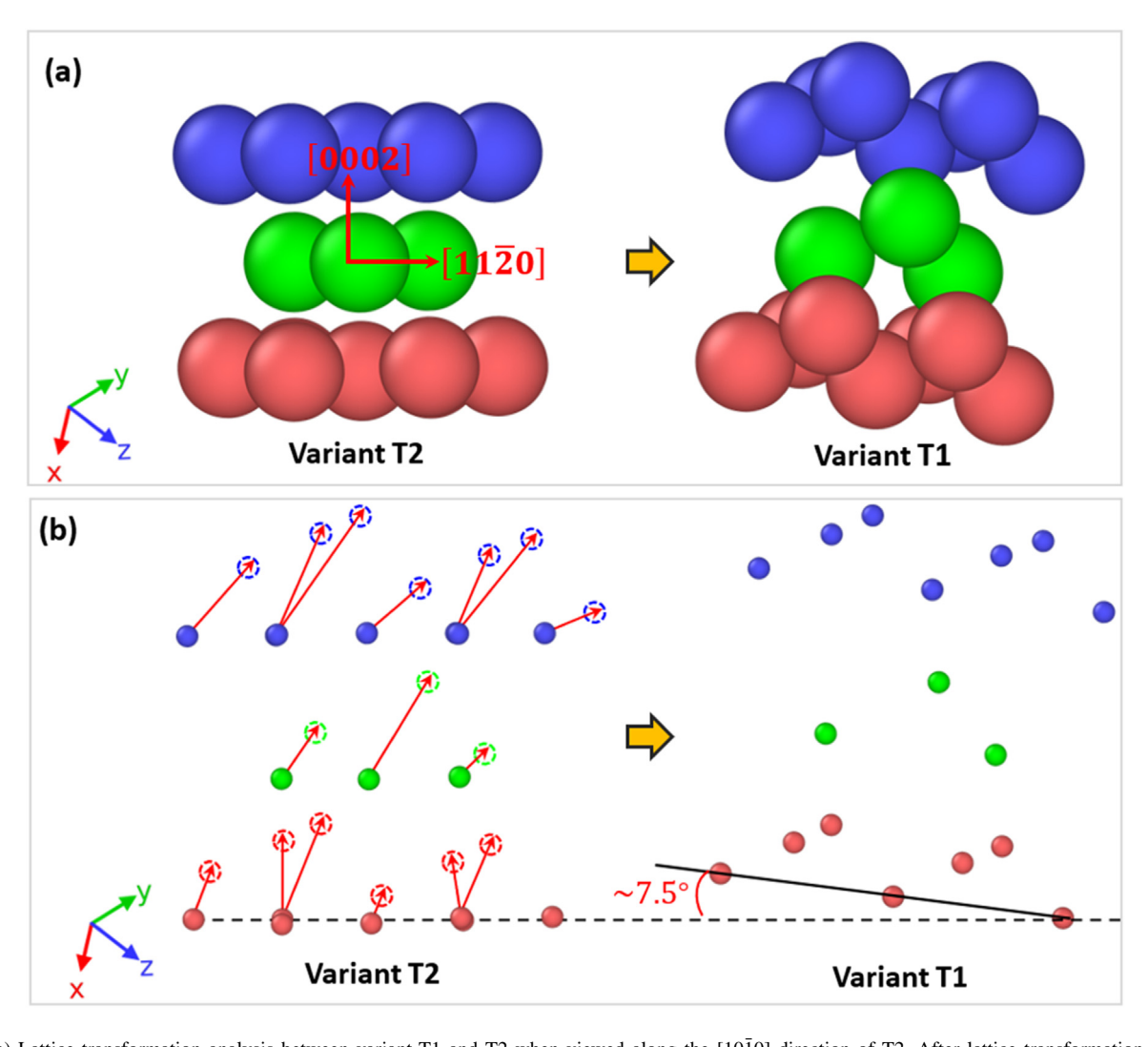


Fig. 10. (a) Lattice transformation analysis between variant-T1 and T2 when viewed along the $[10\overline{1}0]$ direction of T2. After lattice transformation, the lattice of T2 is slightly tilted. (b) The lattice of T1 and T2 are superimposed to show the major atomic displacements from T2 to T1 (indicated by the red arrows). The tilt angle is approximately 7.5° in this viewing direction. The X-Y-Z axes represent the original coordinate system of the single crystal.

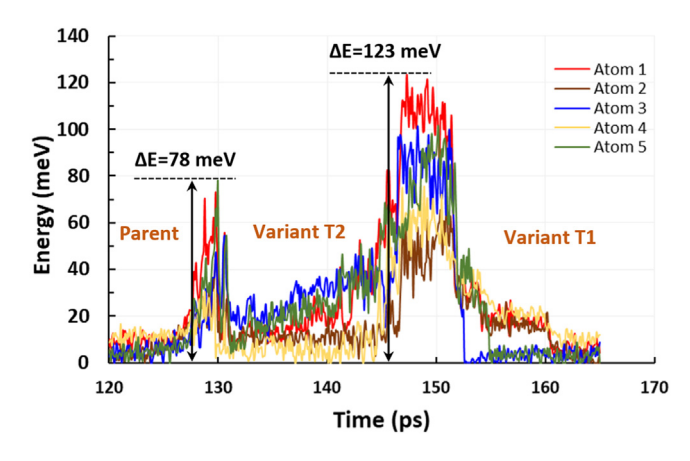


Fig. 11. Evolution of potential energy of five atoms in the unit cell of Fig. 8 during twin-twin interaction. The selected atoms are initially in the parent lattice which is first transformed into variant-T2, and then transformed from T2 into T1. The energy barrier from parent to T2 is \sim 78 meV, and the barrier from T2 to T1 is \sim 123 meV which is significantly higher.

{111} twinning in FCC metals, which is associated with a homogeneous simple shear mediated by twinning dislocations [52]. Song and Gray [65,66] first proposed that $\{10\overline{1}2\}\langle10\overline{1}\overline{1}\rangle$ twin growth was not controlled by twinning dislocations, but by complex atomic movements involving a large number of atoms. Such complex shuffles led to the formation of frequently observed anomalous basal stacking faults inside $\{1012\}\langle 1011\}$ and $\{1011\}\langle 1012\}$ twins in HCP metals [46– 49,67,68]. Li and Zhang [51] analyzed the lattice transformation in $\{10\overline{1}2\}\langle10\overline{1}\overline{1}\rangle$ twinning and showed that the theoretical twinning plane {1012} cannot remain invariant during twinning, thus no twinning dislocation should exist on {1012} twin boundaries. The lack of twinning dislocations in this twinning mode has led to very anomalous twinning behavior that has been observed in extensive experiments and simulations [59,69–71]. For instance, Gharghouri et al. [71] observed that a {1012} twin could change its habit plane when encountered a precipitate and could engulf a precipitate. Recently, using electron backscatter diffraction (EBSD), Mao et al. [72] ana14

lyzed $\{10\bar{1}2\}$ twin-twin interaction in an AZ31 Mg alloy that was deformed at ultra-high strain rate ($\sim 10^6/\text{sec}$) produced by laser shock peening. They found that a twin variant can be totally surrounded by another twin variant, forming isolated twin islands; when two twin variants impinged, a twin variant could grow laterally around the other variant, forming a structure that looked like a variant crossed the other. Such a twin-twin interaction does not involve any twinning dislocations and can be characterized as "soft twin-twin interaction" which contributes insignificantly to work hardening.

4.4. Increase of stress for twin growth during $\{10\overline{1}1\}$ twin-twin interaction

Extensive experimental observations and simulations have shown that the twin-twin interaction contribute to work hardening of materials [18,24,73–75]. Sehitoglu et al. [75] quantitively evaluated the energy barrier of twin-twin interaction and twin-slip interaction in an FCC high entropy alloy, and found that the twin-twin interaction significantly contributed to hardening, while the twin-slip interaction only caused less hardening, even softening. In this work, the interaction between {1011} variants may contribute to work hardening, because: (1) the lengthening of the incoming twin variant T2 is suppressed by the barrier variant T1; (2) although the twinning dislocations of T1 are able to penetrate the twin-twin intersection, the energy barrier to the penetration should be higher than that to the original twinning dislocations on the twin boundary.

To quantitatively determine the hardening effect of twintwin interaction, we compute the evolution of the potential energy of a pre-selected group of atoms in the parent lattice. During deformation, the positions of these atoms are then transformed to the T2 lattice and then to the T1 lattice. Fig. 11 shows the energy profile of five atoms that have the highest energy change. The first energy peak represents the energy barrier to the parent \rightarrow T2 twinning, which has a value of \sim 78 meV. The second energy peak represents the energy barrier to the $T2 \rightarrow T1$ transformation and has a value of \sim 123 meV, significantly higher than the energy barrier to the parent \rightarrow T2, i.e., {1011} twinning. Hence, when a zonal twinning dislocation of T1 is gliding through the parent lattice, it experiences a relatively low energy barrier. When this dislocation impinges on the twin-twin intersection, an extra effort is required for this dislocation to pass through the lattice of T2 and transforms the lattice of T2 into T1. Therefore, the stress for twin growth can be anticipated to be increased during such twin-twin interaction.

As revealed in Fig. 9-10, the T2 \rightarrow T1 lattice transformation is almost identical to that of $\{10\bar{1}2\}\langle10\bar{1}\bar{1}\}\rangle$ twinning, except for the additional tilt. It is worth comparing the energy barrier to the T2 \rightarrow T1 lattice transformation and the barrier to $\{10\bar{1}2\}\langle10\bar{1}\bar{1}\rangle\rangle$ twinning. Wang et al. [60] computed the energy barrier to the shuffling-dominated $\{10\bar{1}2\}\langle10\bar{1}\bar{1}\rangle\rangle$ twin nucleation by using first principles calculations. Their results showed that the energy barrier to the lattice transformation from parent to twin was about \sim 27 meV/atom. Thus, de-

spite that the T2 \rightarrow T1 lattice transformation is very close to that of $\{10\bar{1}2\}\langle10\bar{1}\bar{1}\rangle$ twinning, the additional tilt (Fig. 9-10), which deviates the orientation relationship from $\{10\bar{1}2\}\langle10\bar{1}\bar{1}\rangle$ twinning, significantly increases the energy barrier and contributes to the hardening effect due to the observed twin-twin interaction.

4.5. The correlation between $\{10\bar{1}1\}$ twin-twin interaction and crack nucleation

At high stress levels close to fracture, $\{10\bar{1}1\}$ twinning [26] and the interaction between their variants [20,23,24], as well as $\{10\bar{1}1\} - \{10\bar{1}2\}$ double twinning [76] can occur. Those twinning behaviors are usually correlated to the crack nucleation [23,77]. However, Lentz et al. [21] showed that the presence of $\{10\bar{1}1\}$ twin networks and double twin have almost no reduction on the failure strains in Mg-4 wt.% Li alloy, compared to pure Mg with very limited $\{10\bar{1}1\}$ twins. Similarly, it was reported that the abundant $\{10\bar{1}1\}$ twins in a directionally solidified magnesium alloy can contribute to uniform deformation without initiating early crack [20]. Therefore, the role of contraction twins and their interactions in plastic deformation and fracture failure of Mg alloys needs further investigations.

Twin-twin interaction often introduces stress concentrations due to the lattice mismatch and imped of twinning dislocations. If the stress concentration at the intersections cannot be properly relaxed, crack might be initiated. In this work, we reveal that when two {1011} twin invariants interact, one variant can continue growing at the expense of the other one, due to their lattice transformation is very close to that of {1012}(1011) twinning. Thus, such twin-twin interaction might not be prone for crack nucleation. The crystallographic orientation of the twins, stress state near the junction and plastic relaxation mechanisms are crucial for affecting crack nucleation. Understanding the effect of twin-twin interactions on crack nucleation can provide valuable insights into the designing of Mg alloys with enhanced fracture resistance. Experimental techniques such as in situ mechanical testing and advanced characterization microscopy are necessary for studying twin-twin interactions and their effects on crack nucleation in the future work.

5. Conclusion

In this work, interaction between non-co-zone {1011} twin variants is observed and analyzed. The interaction mechanism is resolved by performing lattice correspondence analyses. The following conclusions can be drawn:

(1) When an incoming {1011} twin variant impinges on the other variant (the barrier twin), the lengthening of the incoming variant is inhibited, but thickening can still occur by nucleating more twinning dislocations on the twin boundaries. The impingement facilitates the nucleation of twinning dislocations of the barrier variant. A twin variant is able to grow at the expense of the other. The twinning

- dislocations are able to pass through the twin-twin intersection and transforms the lattice of a variant into the lattice of the other variant.
- (2) The lattice transformation from a variant to the other is very close to that of $\{10\bar{1}2\}(10\bar{1}\bar{1})$ twinning in HCP metals and involves complex atomic shuffles. However, a deviation from the $\{10\bar{1}2\}$ twin relationship exists. After lattice transformation, the product lattice is slightly tilted and off the $\{10\bar{1}2\}$ twin relationship. The lattice transformation is accomplished by the co-action of a shear mediated by the twinning dislocations and atomic shuffles.
- (3) Although the lattice transformation during twin-twin interaction is essentially similar to that of {1012}(1011) twin, the slight deviation from the twin relationship between the two lattices presents a significant energy barrier for the twinning dislocations to penetrate the twin-twin intersection. Such a dislocation-mediated twin-twin interaction is expected to produce a strong hardening effect during deformation.

Declaration of Competing Interests

The authors declare that they have no known competing financial interests or personal relationships that could have appeared to influence the work reported in this paper.

CRediT authorship contribution statement

Peng Chen: Writing – original draft, Visualization, Validation, Methodology, Investigation, Conceptualization. **Bin Li:** Writing – review & editing, Supervision, Resources, Investigation, Funding acquisition.

Acknowledgements

Bin Li thanks the support from U.S. National Science Foundation (NSF) (CMMI-2016263, 2032483). Peng Chen thanks the support from Program for the Central University Youth Innovation Team and Fundamental Research Funds for the Central Universities, Jilin University.

References

- [1] S. Mahajan, Philos. Mag. J. Theor. Exp. Appl. Phys. 23 (1971) 781–794, doi:10.1080/14786437108216988.
- [2] S. Mahajan, G.Y. Chin, Acta Metall 21 (1973) 173–179, doi:10.1016/ 0001-6160(73)90059-X.
- [3] L. Remy, Scr. Metall. 11 (1977) 169-172.
- [4] K. Rajan, J. Mater. Sci. Lett. 1 (1982) 482–484, doi:10.1007/ BF00721935.
- [5] X.Z. Lv, J.X. Zhang, H. Harada, Int. J. Fatigue. 66 (2014) 246–251, doi:10.1016/j.ijfatigue.2014.04.012.
- [6] S. Alkan, A. Ojha, H. Sehitoglu, Acta Mater 147 (2018) 149–164, doi:10.1016/j.actamat.2017.12.058.
- [7] J.W. Christian, S. Mahajan, Prog. Mater. Sci. 39 (1995) 1-157.
- [8] L. Remy, Metall. Mater. Trans. A. 12 (1981) 387-408.
- [9] M.H. Yoo, J.K. Lee, Philos. Mag. A. 63 (1991) 987-1000.
- [10] P. Chen, B. Li, D. Culbertson, Y. Jiang, Mater. Sci. Eng. A. 709 (2018) 40–45, doi:10.1016/j.msea.2017.10.038.

- [11] M.D. Nave, M.R. Barnett, Scr. Mater. 51 (2004) 881–885, doi:10.1016/j.scriptamat.2004.07.002.
- [12] Q. Yu, J. Wang, Y. Jiang, R.J. McCabe, C.N. Tomé, Mater. Res. Lett. 2 (2014) 82–88, doi:10.1080/21663831.2013.867291.
- [13] K. Yaddanapudi, M.A. Kumar, J. Wang, X. Wang, T.J. Rupert, E.J. Lavernia, J.M. Schoenung, I.J. Beyerlein, S. Mahajan, J. Magnes. Alloys. 11 (2023) 176–191, doi:10.1016/j.jma.2022.11.008.
- [14] Q. Yu, J. Wang, Y. Jiang, R.J. McCabe, N. Li, C.N. Tomé, Acta Mater 77 (2014) 28–42, doi:10.1016/j.actamat.2014.05.030.
- [15] F. Mokdad, D.L. Chen, D.Y. Li, J. Alloys Compd. 737 (2018) 549–560, doi:10.1016/j.jallcom.2017.12.043.
- [16] Q. Ma, H. El Kadiri, A.L. Oppedal, J.C. Baird, B. Li, M.F. Horstemeyer, S.C. Vogel, Int. J. Plast. 29 (2012) 60–76, doi:10.1016/j.ijplas.2011.08. 001
- [17] Q. Sun, X.Y. Zhang, Y. Ren, L. Tan, J. Tu, Mater. Charact. 109 (2015) 160–163, doi:10.1016/j.matchar.2015.09.024.
- [18] P. Chen, F. Wang, J. Ombogo, B. Li, Mater. Sci. Eng. A. 739 (2019) 173–185, doi:10.1016/j.msea.2018.10.029.
- [19] M.H. Yoo, Metall. Trans. A. 12 (1981) 409–418, doi:10.1007/ BF02648537.
- [20] X. Lin, T. Zhao, Y. Dong, J. Ye, Z. Fan, H. Xie, L. Wang, Mater. Sci. Eng. A. 700 (2017) 681–689, doi:10.1016/j.msea.2017.06.053.
- [21] M. Lentz, M. Risse, N. Schaefer, W. Reimers, I.J. Beyerlein, Nat. Commun. 7 (2016) ncomms11068, doi:10.1038/ncomms11068.
- [22] L. Jiang, J.J. Jonas, R.K. Mishra, A.A. Luo, A.K. Sachdev, S. Godet, Acta Mater 55 (2007) 3899–3910, doi:10.1016/j.actamat.2007.03.006.
- [23] J. Singh, M.-S. Kim, S.-H. Choi, J. Alloys Compd. 708 (2017) 694–705, doi:10.1016/j.jallcom.2017.02.176.
- [24] H. Li, Q. Zeng, P. Yang, Q. Sun, J. Wang, J. Tu, M. Zhu, J. Mater. Sci. Technol. 43 (2020) 230–237, doi:10.1016/j.jmst.2020.01.007.
- [25] Q. Zhang, J. Li, K. Jiang, P. Li, Y. Li, Y. Zhang, T. Suo, J. Magnes. Alloys. 11 (2023) 2872–2882, doi:10.1016/j.jma.2021.10.014.
- [26] Y.M. Zhu, S.W. Xu, J.F. Nie, Acta Mater 143 (2018) 1–12, doi:10.1016/j.actamat.2017.09.067.
- [27] B. Li, E. Ma, Acta Mater 57 (2009) 1734–1743, doi:10.1016/j.actamat. 2008.12.016.
- [28] Y. Yue, J. Wang, J.-F. Nie, J. Magnes. Alloys. 11 (2023) 3427–3462, doi:10.1016/j.jma.2023.07.015.
- [29] Q. Peng, Y. Sun, J. Wang, Q. Zu, M. Yang, H. Fu, Acta Mater (2020), doi:10.1016/j.actamat.2020.03.035.
- [30] A. Chakkedath, C.J. Boehlert, JOM 67 (2015) 1748–1760, doi:10.1007/ s11837-015-1478-5.
- [31] M.S. Daw, M.I. Baskes, Phys. Rev. Lett. 50 (1983) 1285–1288, doi:10. 1103/PhysRevLett.50.1285.
- [32] M.S. Daw, M.I. Baskes, Phys. Rev. B. 29 (1984) 6443–6453, doi:10. 1103/PhysRevB.29.6443.
- [33] X.-Y. Liu, J.B. Adams, F. Ercolessi, J.A. Moriarty, Model. Simul. Mater.
- Sci. Eng. 4 (1996) 293, doi:10.1088/0965-0393/4/3/004.

 [34] D.Y. Sun, M.I. Mendelev, C.A. Becker, K. Kudin, T. Haxhimali,

 M. Asto, I.I. Hout, A. Kormo, D.I. Szolovitz, Phys. Rev. B 73 (2006)
- M. Asta, J.J. Hoyt, A. Karma, D.J. Srolovitz, Phys. Rev. B. 73 (2006) 024116, doi:10.1103/PhysRevB.73.024116.
- [35] M.I. Baskes, R.A. Johnson, Model. Simul. Mater. Sci. Eng. 2 (1994) 147, doi:10.1088/0965-0393/2/1/011.
- [36] Y.-M. Kim, N.J. Kim, B.-J. Lee, Calphad 33 (2009) 650–657, doi:10. 1016/j.calphad.2009.07.004.
- [37] Z. Wu, M.F. Francis, W.A. Curtin, Model. Simul. Mater. Sci. Eng. 23 (2014) 015004, doi:10.1088/0965-0393/23/1/015004.
- [38] P. Chen, F. Wang, B. Li, Acta Mater 164 (2019) 440–453, doi:10.1016/j.actamat.2018.10.064.
- [39] B. Li, E. Ma, Philos. Mag. 89 (2009) 1223–1235, doi:10.1080/ 14786430902936707.
- [40] P. Chen, F. Wang, B. Li, Comput. Mater. Sci. 164 (2019) 186–194, doi:10.1016/j.commatsci.2019.04.020.
- [41] W.G. Hoover, Phys. Rev. A. 31 (1985) 1695–1697, doi:10.1103/ PhysRevA.31.1695.
- [42] S. Nosé, J. Chem. Phys. 81 (1984) 511-519, doi:10.1063/1.447334.
- [43] A. Stukowski, Model. Simul. Mater. Sci. Eng. 18 (2010) 015012, doi:10. 1088/0965-0393/18/1/015012.

- 16
- [44] S. Plimpton, J. Comput. Phys. 117 (1995) 1–19, doi:10.1006/jcph.1995.
- [45] J.Dana. Honeycutt, H.C. Andersen, J. Phys. Chem. 91 (1987) 4950–4963, doi:10.1021/j100303a014.
- [46] B. Li, Q. Sun, X.Y. Zhang, Comput. Mater. Sci. 198 (2021) 110684, doi:10.1016/j.commatsci.2021.110684.
- [47] S.G. Song, G.T.G. III, Philos. Mag. A. 71 (1995) 263–274, doi:10.1080/ 01418619508244355.
- [48] X.Y. Zhang, B. Li, Q. Liu, Acta Mater. 90 (2015) 140–150, doi:10. 1016/j.actamat.2015.02.036.
- [49] X.Y. Zhang, B. Li, J. Tu, Q. Sun, Q. Liu, Mater. Res. Lett. 3 (2015) 142–148, doi:10.1080/21663831.2015.1034297.
- [50] Q. Sun, Q. Zhang, B. Li, X. Zhang, L. Tan, Q. Liu, Scr. Mater. 141 (2017) 85–88, doi:10.1016/j.scriptamat.2017.07.036.
- [51] B. Li, X.Y. Zhang, Scr. Mater. 125 (2016) 73–79, doi:10.1016/j. scriptamat.2016.07.004.
- [52] B.A. Bilby, A.G. Crocker, Proc. R. Soc. Lond. Ser. Math. Phys. Sci. 288 (1965) 240–255, doi:10.1098/rspa.1965.0216.
- [53] X. Li, J. Li, B. Zhou, M. Yu, M. Sui, J. Mater. Sci. Technol. 35 (2019) 660–666, doi:10.1016/j.jmst.2018.09.049.
- [54] D. Hull, D.J. Bacon, Introduction to Dislocations, Fifth Edition, 5 edition, Butterworth-Heinemann, Amsterdam, 2011.
- [55] A.W. Sleeswyk, C.A. Verbraak, Acta Metall 9 (1961) 917–927, doi:10. 1016/0001-6160(61)90110-9.
- [56] J.W. Christian, Newnes (2002).
- [57] Z.S. Basinski, M.S. Szczerba, M. Niewczas, J.D. Embury, S.J. Basinski, Rev. Métallurgie. 94 (1997) 1037–1044, doi:10.1051/metal/199794091037.
- [58] M. Niewczas, Acta Mater 58 (2010) 5848–5857, doi:10.1016/j.actamat. 2010.06.059.
- [59] B. Li, E. Ma, Phys. Rev. Lett. 103 (2009) 035503, doi:10.1103/ PhysRevLett.103.035503.
- [60] J. Wang, S.K. Yadav, J.P. Hirth, C.N. Tomé, I.J. Beyerlein, Mater. Res. Lett. 1 (2013) 126–132, doi:10.1080/21663831.2013.792019.
- [61] P. Chen, J. Ombogo, B. Li, Acta Mater 186 (2020) 291–307, doi:10. 1016/j.actamat.2020.01.010.

- [62] K. Fukuda, Y. Koyanagi, M. Tsushida, H. Kitahara, T. Mayama, S. Ando, Mater. Trans. 58 (2017) 587–591, doi:10.2320/matertrans. M2016402.
- [63] J.P. Hirth, J. Lothe, Theory of Dislocations, 2nd (second) Edition, Krieger Publishing Company, 1983.
- [64] S. Mendelson, Mater. Sci. Eng. 4 (1969) 231–242, doi:10.1016/ 0025-5416(69)90067-6.
- [65] S.G. Song, G.T. Gray, Acta Metall. Mater. 43 (1995) 2339–2350, doi:10. 1016/0956-7151(94)00434-X.
- [66] S.G. Song, G.T. Gray, Acta Metall. Mater. 43 (1995) 2325–2337, doi:10. 1016/0956-7151(94)00433-1.
- [67] B. Li, Q.W. Zhang, S.N. Mathaudhu, Scr. Mater. 134 (2017) 37–41, doi:10.1016/j.scriptamat.2017.02.040.
- [68] B. Zhou, M. Sui, J. Mater. Sci. Technol. 35 (2019) 2263–2268, doi:10. 1016/j.jmst.2019.05.042.
- [69] B.-Y. Liu, J. Wang, B. Li, L. Lu, X.-Y. Zhang, Z.-W. Shan, J. Li, C.-L. Jia, J. Sun, E. Ma, Nat. Commun. 5 (2014), doi:10.1038/ ncomms4297.
- [70] P.G. Partridge, E. Roberts, Acta Metall 12 (1964) 1205–1210, doi:10. 1016/0001-6160(64)90103-8.
- [71] M.A. Gharghouri, G.C. Weatherly, J.D. Embury, Philos. Mag. A. 78 (1998) 1137–1149, doi:10.1080/01418619808239980.
- [72] B. Mao, Y. Liao, B. Li, Scr. Mater. 165 (2019) 89–93, doi:10.1016/j. scriptamat.2019.02.028.
- [73] H. El Kadiri, J. Kapil, A.L. Oppedal, L.G. Hector, S.R. Agnew, M. Cherkaoui, S.C. Vogel, Acta Mater 61 (2013) 3549–3563, doi:10. 1016/j.actamat.2013.02.030.
- [74] M. Arul Kumar, M. Gong, I.J. Beyerlein, J. Wang, C.N. Tomé, Acta Mater 168 (2019) 353–361, doi:10.1016/j.actamat.2019.02.037.
- [75] M. Bönisch, Y. Wu, H. Sehitoglu, Acta Mater 153 (2018) 391–403, doi:10.1016/j.actamat.2018.04.054.
- [76] J. Jain, J. Zou, C.w. Sinclair, W.j. Poole, J. Microsc. 242 (2011) 26–36, doi:10.1111/j.1365-2818.2010.03434.x.
- [77] S. Niknejad, S. Esmaeili, N.Y. Zhou, Acta Mater 102 (2016) 1–16, doi:10.1016/j.actamat.2015.09.026.